Stable lithium-ion batteries based on a hybrid aqueous/organic electrolyte

Journal of Power Sources 612 (2024) 234803

Contents lists available at ScienceDirect

Journal of Power Sources

journal homepage: www.elsevier.com/locate/jpowsour

Stable lithium-ion batteries based on a hybrid aqueous/organic electrolyte

Shahid Khalid [a], Ivan Claudio Pellini [a], Nicolò Pianta [a], Roberto Lorenzi [a], Silvia Leonardi [b], Laura Meda [b], Caterina Rizzo [c], Ernesto Roccaro [c], Patrik Johansson [d,e], Piercarlo Mustarelli [a,f], Riccardo Ruffo [a,f,*]

[a] Department of Materials Science, University of Milano-Bicocca, Via Cozzi 55, 20125, Milano, Italy
[b] ENI DE-R&D, Via Fauser 4, 28100, Novara, Italy
[c] ENI DE-R&D, Via Felice Maritano 26, 20097, S. Donato M.se, Italy
[d] Department of Physics, Chalmers University of Technology, SE-41296, Göteborg, Sweden
[e] Alistore-ERI, CNRS FR 3104, 15 Rue Baudelocque, 80039, Amiens, France
[f] National Reference Center for Electrochemical Energy Storage (GISEL), Consorzio Interuniversitario Nazionale per la Scienza e Tecnologia dei Materiali (INSTM), 50121, Firenze, Italy

HIGHLIGHTS

- Three-component electrolytes with sulfolane, water and lithium salt were studied.
- The highest concentrated electrolyte is coupled with LTO and LMO as the anode and the cathode.
- The cell shows has excellent cycling stability and safety.
- The interactions among the different components were studied by solvation models.

ARTICLE INFO

Keywords:
Water in salt
Hybrid electrolytes
Sulfolane
Solvation structure
LiFTFSI

ABSTRACT

Moving from organic to aqueous lithium-ion batteries (ALIBs) would be an interesting feat. As of today, we have water-in-salt electrolytes (WISEs) that were developed primarily to expand the electrochemical stability window of traditional aqueous electrolytes. However, their cathodic limits do not enable the use of high-capacity negative electrodes and the very high concentrations of expensive heavily fluorinated salts, often >20 mol kg^{-1}, hinder any feasible implementation of LIBs based on WISEs. A hybrid organic/aqueous electrolyte based on LiFTFSI dissolved in sulfolane and water is here presented as an alternative, where sulfolane is used to tune and reduce the water activity, by altering the Li^+ cation first solvation shell, and thereby the cathodic limit can be pushed to <1.0 V *vs.* Li^+/Li even at a comparatively moderate salt concentration (7.8 mol kg^{-1}). This enables long-term operation of an $Li_4Ti_5O_{12}$ | hybrid electrolyte | $LiMn_2O_4$ 2.4 V cell with a specific energy of 156 Wh kg_{AM}^{-1}.

1. Introduction

Aqueous lithium-ion batteries (ALIBs) have the potential to offer safety advantages and lower cost as compared to traditional LIBs [1,2], but most often their energy densities are severely limited by the narrow electrochemical stability window (ESW) of the water employed in the electrolytes [3]. As a remedy, highly concentrated aqueous electrolytes (water-in-salt electrolytes or WISEs) have been introduced, that significantly extend the ESW from the conventional *ca.* 1.23 V to >3 V due to a combination of bulk, interfacial, and interphase effects [4]. Indeed, "superconcentration" influences water activity and changes the solvation structure by incorporating almost all water molecules and some salt anions into the (Li^+) cation first solvation shells, resulting in overpotentials for water decomposition [4–7]. Furthermore, the preferential reduction of the Li-salt anions over water in WISEs leads to the formation of different and more stable solid electrolyte interphases (SEIs) on the negative electrode surface, significantly increasing the cathodic stability [8], but this is heavily dependent on the use of perfluorinated anions [5,9–11]. The accumulation of anionic species at the surface of the positive electrode, creating a water-depleted region, also increases

* Corresponding author. Department of Materials Science, University of Milano-Bicocca, Via Cozzi 55, 20125, Milano, Italy.
E-mail address: riccardo.ruffo@unimib.it (R. Ruffo).

https://doi.org/10.1016/j.jpowsour.2024.234803
Received 15 March 2024; Received in revised form 30 April 2024; Accepted 27 May 2024
Available online 4 June 2024

the oxidative stability [8]. However, the cathodic stability of WISEs is not yet sufficient to support even rather high potential and high-capacity commercial LIB negative electrodes, such as $Li_4Ti_5O_{12}$ (LTO) operating at *ca.* 1.5 V *vs.* Li^+/Li, and in addition, the substantial salt concentrations required raise significant economic concerns alongside elevated viscosities, posing practical challenges [12]. An alternative is to create hybrid aqueous/organic electrolytes (bi-solvent-in-salt-electrolytes or BSiSEs), where the organic component both improves the SEI [13,14] and the cathodic stability by replacing the cation coordinated water molecules with an electrochemically more stable co-solvent. This effectively hinders solvated water molecules from migrating into the inner Helmholtz layer, which would trigger the hydrogen evolution reaction (HER) [15,16]. Several co-solvents have been successfully employed: dimethyl carbonate [13], acetonitrile [17], tetraethylene glycol dimethyl ether (TEGDME), and 1,3-dioxolane [18,19], and very recently sulfolane which improves the ESW by breaking the hydrogen bond network rather than by stabilizing the SEI itself [20–22]. All the BSiSEs above use salt concentrations >10 mol kg^{-1}, which while admittedly is only 50 % of most WISEs, this is still high and using a co-solvent may allow less expensive electrolytes, even if perfluorinated anions are employed.

Despite the large amount of literature on the various approaches, there are still a number of unresolved practical issues relating to the actual development of these technologies. In particular, due to the corrosive properties of superconcentrated electrolytes, titanium current collectors are often used, which are expensive and of little practical use. In addition, as mentioned above, the use of highly concentrated perfluorinated salts poses problems in terms of both cost and environmental sustainability.

In this work, we report the use of water containing electrolytes with sulfolane as co-solvent and LiFTFSI as salt. The asymmetric FTFSI anion was chosen as it has been demonstrated to inhibit crystallization in concentrated electrolytes, as compared to similar electrolytes based on the more common symmetric anions such as TFSI and FSI [23]. In particular, we studied the properties of three different solutions by keeping the sulfolane/water ratio constant (3:1) and varying that of the salt until a maximum solubility of 7.8 mol kg^{-1} was reached. This limit is lower than that which defines a BSiSE, but this is an advantage in terms of cost and sustainability, considering the use of fluorinated salts. We commence our analysis by thoroughly characterizing the physicochemical properties, with a particular focus on thermal and phase characteristics, before delving into the evaluation of electrochemical properties. Subsequently, the prospect of these electrolytes for ALIBs is demonstrated by constructing a $Li_4Ti_5O_{12}$ (LTO)|electrolyte|$LiMn_2O_4$ (LMO) full cell on standard current collectors.

2. Methods

2.1. Electrolyte preparation

The electrolytes were prepared by mixing LiFTSFI (>97 %, TCI), sulfolane (99 %, Sigma Aldrich) and Milli-Q water ($\sigma = 6.3$ μS cm^{-1}). Keeping the sulfolane/water ratio constant at 3:1 and changing the molar ratio of LiFTFSI respect to water from 1 to 3, three samples were obtained, namely 3S:H_2O:1L, 3S:H_2O:2L, and 3S:H_2O:3L. All the samples were stirred for 30 min to ensure complete dissolution of the salt, then stored and used at room temperature.

2.2. Thermal studies

Thermal characterization of the electrolyte samples was done with Differential Scanning Calorimetry (DSC) using DSC 1 Star® (Mettler Toledo). The data was evaluated using STARe® software. Thermal analysis was performed in a temperature range of −120 to 80 °C. The experimental protocol included four steps: 1) equilibration at 25 °C for 10 min; 2) cooling from 25 °C to −120 °C at 5 °C/min; 3) isotherm at −120 °C for 10 min; 4) heating from −120 °C to 80 °C at 5 °C/min.

2.3. Conductivity measurement

The conductivity was measured using electrochemical impendence spectroscopy in the frequency range 1 Hz–400 kHz, with a sine amplitude of 25 mV, using a dip-probe symmetric platinum electrode cell having a cell constant of 1.06 cm^{-1}. Impedance spectra were obtained vs. temperature in the range of 0 °C–75 °C using a climatic chamber (Angelantoni, Italy) and the bulk ohmic resistance was determined through the high-frequency intercept with x-axis of the Nyquist plots.

2.4. Raman studies

Raman analysis was performed with a Labram Dilor spectrometer (JobinYvon) in backscattering mode using a 488 nm Ar^+ laser having a resolution of 2 cm^{-1}. The laser beam was focused on a circular point through a microscope with a long working distance objective lens having 50× magnification and an aperture of 0.60. The spectra were obtained by accumulating three acquisitions (30 s of integration). All the measurements were performed at room temperature.

2.5. Electrochemical studies

The electrochemical measurements included cyclic voltammetry (CV), linear sweep voltammetry (LSV) and galvanostatic charge/discharge with potential limitation (GCPL). The CV measurements were performed in a three-electrodes Swagelok cell using LTO on Al and LMO on carbon-coated Al (CC–Al) foil as working electrodes (WE, see below) and free-standing activated carbon (F400) and silver/silver chloride (Ag/AgCl, 3.5 KCl) as counter (CE) and reference (RE) electrodes, respectively. All the CV measurements were performed at room temperature with a scan rate of 0.5 mV s^{-1}. The LSV measurements were carried out in a three-electrodes Swagelok cell using Al, CC-Al and stainless steel (SS) foils as WE, and free-standing activated carbon (F400) and silver/silver chloride (Ag/AgCl, 3.5 KCl) as CE and RE, respectively. The scan rate was set the 0.5 mV s^{-1} from 0.0 V vs. RE up to −2.5 V and 2.0 V vs. RE during the cathodic and anodic polarizations, respectively. GCPL measurements were performed in R2032 coin cells at room temperature. For the LMO and LTO electrodes, a slurry of active materials ($LiMn_2O_4$, $Li_4Ti_5O_{12}$), PVDF (6020 by Solvay) binder and carbon black (Super P from Erachem Comilog, Inc.) in weight ratio 8:1:1 was prepared in anhydrous N-methyl-2-pyrrolidone and coated on carbon-coated Al (for LMO) and pristine Al foil (LTO). LMO and LTO electrodes mass loading was 6.7 and 5.2 mg cm^{-2}, respectively. Glass microfilter separator was used in all measurements and 50 μl–70 μl of electrolyte was used in the coin cells. The round trip efficiency is defined as:

$$round\ trip\ efficieny = \frac{E_d}{E_c}\%$$

where E_d is the energy retrieved from the battery when it's discharged and E_c is the energy stored in it when it was charged.

2.6. ARC measurements

Accelerated Rate Calorimetry (ARC) tests were performed using an ES-ARC instrument (THT Ltd., UK). Two coin cells, both assembled with LTO as anode, LMO as cathode, glass microfiber (Whatman) as separator, with the only difference in the electrolyte (LP30 or 3S:H_2O:3L, respectively) were charged up to 2.5V and then tested in the ARC. The experimental procedure, as depicted in the SI (Fig. S10), involves incremental heating in 5 °C steps, followed by 10-min isotherm intervals to ensure thermal equilibrium across the entire chamber. Subsequently, the temperature is monitored for an additional 10 min to allow for

potential exothermal processes. In the absence of observed exothermal reactions, the temperature is increased by another 5 °C, restarting the loop. If an exothermal process is detected, the chamber's temperature is adjusted to match that of the cell.

3. Results and discussion

3.1. Physico-chemical characterization

Three BSiSEs were prepared by keeping the molar ratio between sulfolane and water (3S:H_2O) constant while varying the salt concentration XL (3S:H_2O:XL where X = 1,2,3). First, using DSC to assess phase changes, we find glass transition temperatures (T_gs) in the range −70 to −100 °C (Fig. 1a and S1, Table 1). The T_gs increase as a function of salt content, likely due to dynamic cross-linking by ionic interactions [24], and there is also an increased endothermic overshoot, due to structural relaxation [25]. The most concentrated electrolyte (3S:H_2O:3L) thus requires more energy to move from the glassy to the viscous liquid state and has an intrinsic lower mobility. As no other thermal features, such as cold crystallization or melting, were observed the electrolytes do remain in a supercooled liquid state – which arguably is an advantage in terms of battery cell cycling stability [23].

The ionic conductivities decrease as a function of salt concentration, probably due to increased viscosity, and follow a Vogel-Tammann-Fulcher (VTF) behavior (Fig. 1c) as described by:

$$\sigma = \sigma_o \exp\left(\frac{-B}{T - T_0}\right) \quad \text{(eq.1)}$$

where σ_o is the ionic conductivity at infinite temperature, B is the pseudo activation energy (E_{pa}=$k_B B$, k_B is the Boltzmann constant) for ionic motion, T is the absolute temperature, and T_0 is a parameter relatable to the ideal glass transition temperature [26] at infinitely low heating/cooling rate (thermodynamic equilibrium) [27]. For polymer electrolytes and ionic liquids, T_0 is typically 10–50 °C below T_g due to decoupling from the liquid relaxation and in this case, it is 12–18 °C below T_g, and increases with salt concentration.

The ESWs, as obtained by linear voltammetry (LSV) using either AISI-304 stainless steel (SS), aluminum (Al), or commercial carbon-coated aluminum (CC–Al) as current collectors show that Al gives the best result (Fig. S2) in terms of cathodic stability, probably due to the high overpotential for the HER [28], while the anodic limit is very different between the bare metals (Al, SS) and CC-Al, probably due to metal dissolution. Using the optimized pair of current collectors (Fig. 1b), the cathodic current remains below the threshold of 0.05 mA cm^{-2} up to −2.4 V *vs.* Ag/AgCl, with a trend inversely proportional to the salt concentration. The least concentrated electrolyte, however, shows significantly worse anodic stability. The here introduced use of Al-based current collectors is a breakthrough innovation, as previously only high cost and high specific weight titanium current collectors have provided the anodic stability needed for ALiBs [6,21,22].

Using the 3S:H_2O:3L electrolyte, the lithiation of LTO occurs at −1.64 V *vs.* Ag/AgCl and the corresponding de-lithiation at −1.20 V *vs.* Ag/AgCl (Fig. 1d). Similarly, for LMO, two redox pairs appear at +1.17/+1.34 V *vs.* Ag/AgCl and +0.89/+1.07 V *vs.* Ag/AgCl. All the redox reactions are thus just barely within the ESW of the electrolyte (Fig. 1c).

3.2. Full cell performance

From the basic electrochemistry results above, a set of 2032-type coin cells were fabricated: Al|LTO|3S:H_2O:XL|LMO|CC-Al, with active material loadings >5.0 mg cm^{-2} and an electrolyte volume of 50 µl. Possible future scale-up and transfer to higher TRLs are facilitated both by the use of relevant loadings and conventional current collectors. All cells were subjected to galvanostatic cycling in the potential range between 2.0 and 2.8 V using a rate capability test protocol of different currents, 10 cycles at each, corresponding to 0.5C, 1.0C, 2.0C and 4.0C, and back to 0.5C, where 1C = 150 mA g_{LTO}^{-1} (0.78 mA cm_{LTO}^{-2}). Another

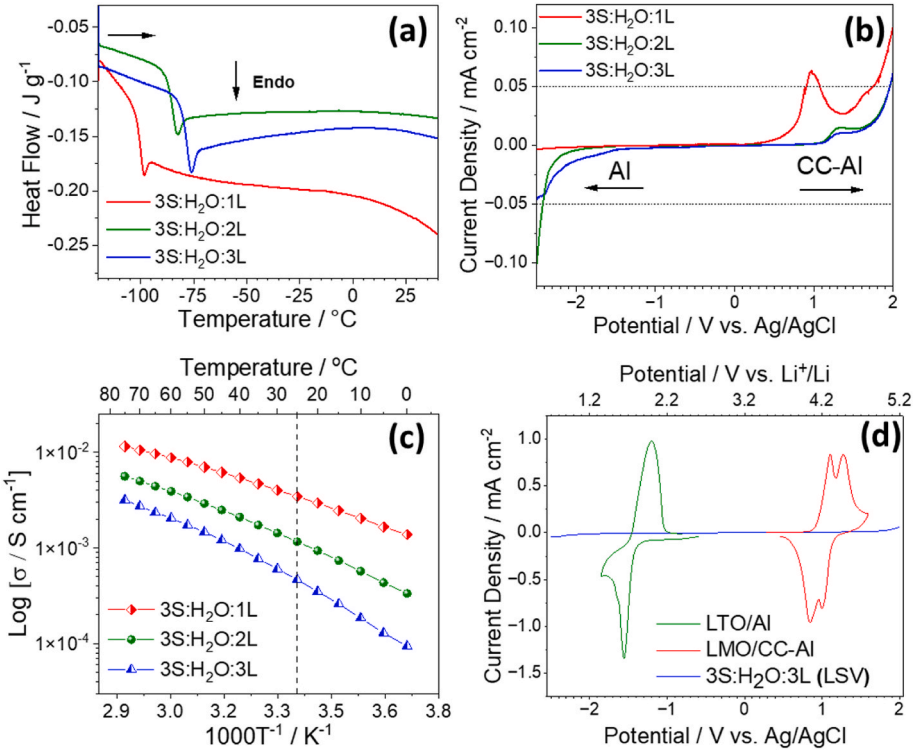

Fig. 1. Characterization of the three electrolytes: (a) DSC traces during heating; (b), Electrochemical stability windows obtained using Al ans Al-CC current collectors during the cathodic and anodic scan, respectively; (c) ionic conductivity as a function of temperature; (d), Cyclic Voltammetry of Al/LTO and Al-CC/LMO electrodes using the 3S:H_2O:3L electrolyte and comparison with the LSV data of Fig. 1b.

Table 1
Physicochemical properties of the hybrid electrolytes.

Electrolyte	Sulfolane:H_2O:LiFTFSI Molar ratio	Molality mol kg^{-1}	Density g mL^{-1}	T_g °C	T_0 °C	T_g-T_0 °C	σ_{RT} mS cm^{-1}	E_{pa} eV
3S:H_2O:1L	3:1:1	2.6	1.35	−98	−116	18	3.5	0.056
3S:H_2O:2L	3:1:2	5.2	1.53	−83	−100	17	1.2	0.060
3S:H_2O:3L	3:1:3	7.8	1.78	−76	−88	12	0.5	0.063

Molality = mol of salt over kg of solvent; T_g from DSC; T_0 from VTF fit; s_{RT} from conductivity measurements, E_{pa} from VTF fit.

set of coin cells was used for the long-term galvanostatic cycling (1000 cycles) at 0.5C (0.39 mA cm^{-2}_{LTO}).

The 3S:H_2O:1L electrolyte, with its modest stability (Fig. 1b), exhibits large irreversibility during the first two charge/discharge cycles (<65 %, Fig. S3), which is why no further cycling was carried out. In contrast, the cells with the two more concentrated electrolytes showed similar performance at 0.5C (Fig. 2a and S4) during the first 50 cycles, with an average discharge potential of 2.4 V and specific capacities of *ca.* 140 mAh g^{-1}_{LTO}. However, after *ca.* 70 cycles, the 3S:H_2O:2L based cell showed a significant drop in performance, resulting in a capacity retention of 89 % and 38 % after 100 and 500 cycles, respectively, while the 3S:H_2O:3L based cell showed 100 % and 78 % (Figures S4, S5 and S6). For the latter, the average charge efficiency between cycles 100 and 1000 was 99.58 ± 0.08 % and at cycle 1000 the capacity retention was 65 % with a loss per cycle of 0.055 mAh g^{-1}. The high active material loading, the good specific capacity, and the high discharge potential result in an initial areal energy density of 1.30 mWh cm^{-2} decreasing to 1.00 and 0.79 mWh cm^{-2} at cycles 500 and 1000, respectively (Fig. 2c). The round-trip efficiency calculated from cycle 2 to 1000 was 90.4 ± 0.5 %. In addition, the rate capability is quite acceptable at 1C and 2C (108 and 69 mAh g^{-1} respectively), while at 4C it dropped down to 20 mAh g^{-1}, but not irreversibly (Fig. 2b).

This improved stability for the cell with the 3S:H2O:3L as compared to 3S:H_2O:2L electrolyte cannot be explained by the simple LSV measurements (Fig. 1b), but LMO induced electrolyte oxidation may play a role. To better understand these aspects detailed Raman characterization was performed to reveal the interactions present, with special emphasis on the cation solvation.

3.3. Cation solvation

The Raman spectral region 500-600 cm^{-1} contains the characteristic SO_2 scissoring vibrational mode of sulfolane (568 cm^{-1}) [29], as also supported by DFT calculations [30], a mode which is known to shift to higher wavenumbers upon complexation with either water or Li^+ [22,31]. Here, the slight shift to 570 cm^{-1} in the 3S:H_2O spectrum became more pronounced as LiFTFSI was introduced; the mode gradually shifted from 572 via 573 to finally reach 574 cm^{-1} for 3S:H_2O:1L, 3S:H_2O:2L, and 3S:H_2O:3L, respectively (Fig. 3a). The latter indicates that almost all sulfolane molecules are now coordinated by Li^+ [21,29]. This spectral region also contains other bands, originating either in the anion, such as the δ_{as}-CF_3 bending mode (556 cm^{-1}) [32], which simply increased in intensity as a function of salt concentration, and/or from both the anion and the sulfolane, such as the broad feature at 510-540 cm^{-1} which is related both to the sulfolane ring deformation mode at *ca.* 516-520 cm^{-1} [30] and an FTFSI combined δ_{as}-CF_3+δ-SO_2 bending vibration mode at *ca.* 535 cm^{-1} [32].

The broad feature in the region 700-800 cm^{-1} is deconvoluted into: (i) a band at 737 cm^{-1} attributed the C–S–C asymmetric stretching of free sulfolane molecules [33,34], (ii) a band around 760 cm^{-1} that correspond to a combination of CF_3-bending and SF-stretching of the FTFSI anion [32], and (iii) a band at 729 cm^{-1} due to contraction/expansion of the full anion [32] (Fig. 3b–Table S1), which, in the presence of solvents, depending on the salt concentration, can give

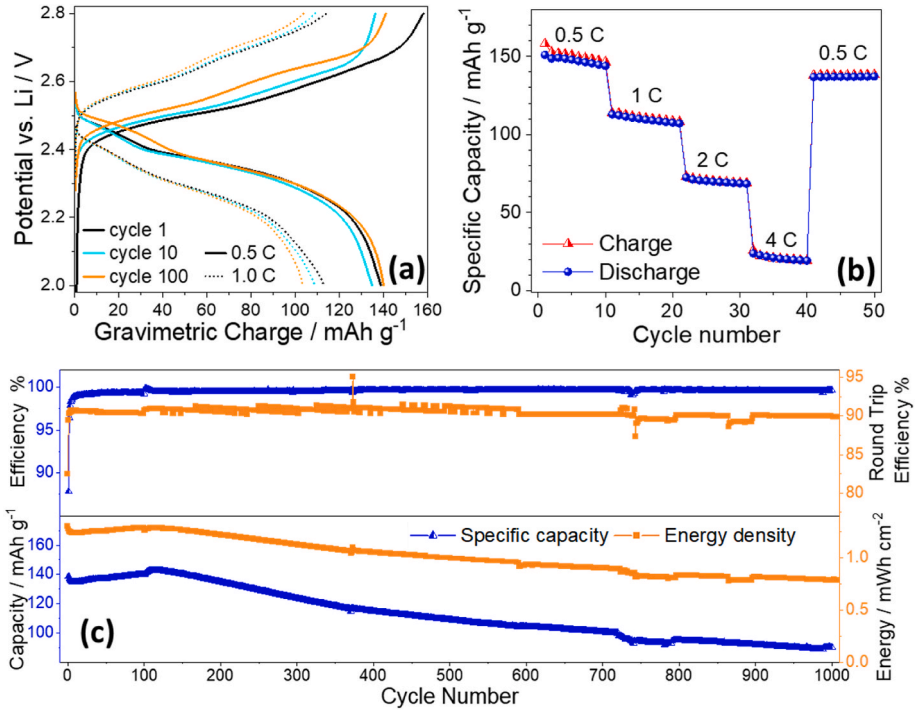

Fig. 2. Galvanostatic charge/discharge profiles at 1C (150 mA g^{-1}) and 0.5C (a), rate capability test (b), and long cycling (c), of the Al|LTO|3S:H_2O:3L|LMO|CC-Al full cell.

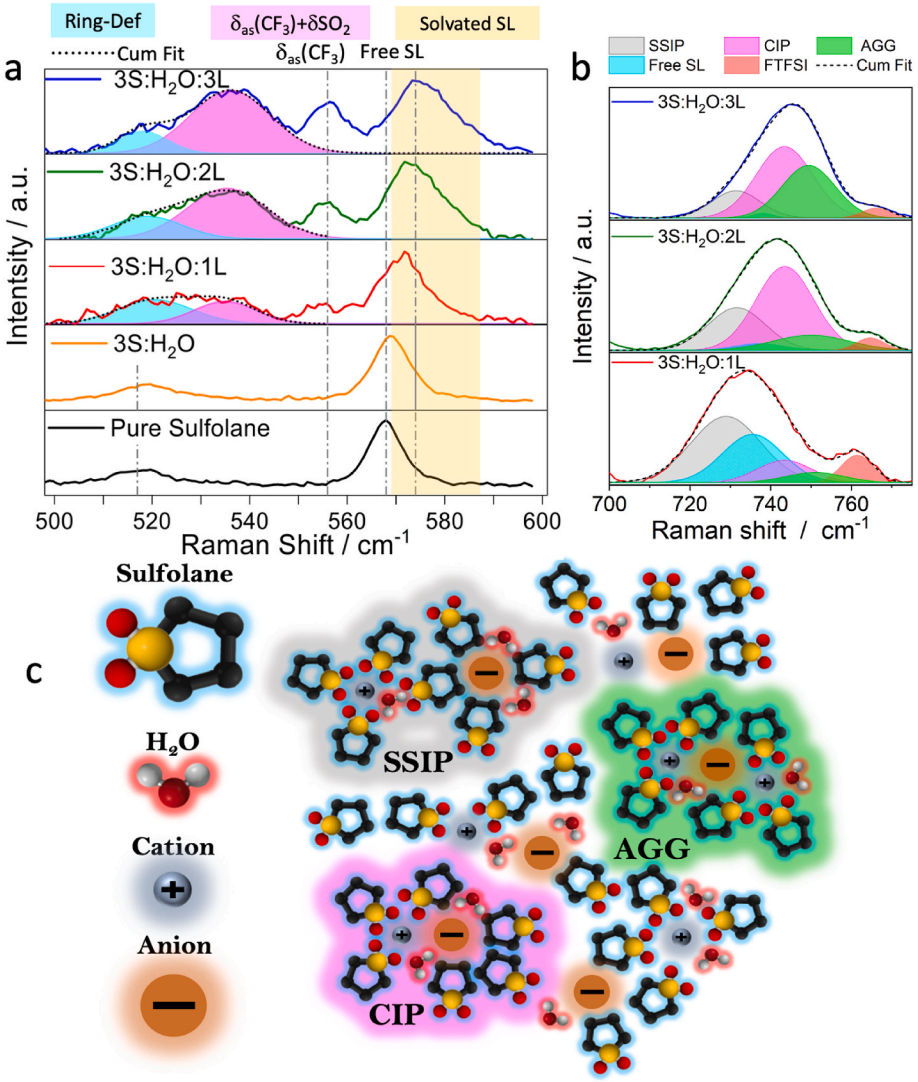

Fig. 3. Raman spectra in the (a) 500–600 and (b) 700–800 wavenumber regions. (c) Sketch of different solvation interactions: SSIP = solvent-separated ion-pair, CIP = contact ion-pair; AGG = aggregate.

rise to various solvation structures, such as: solvent-separated ion-pairs (SSIPs, ~730 cm^{-1}), contact ion-pairs (CIPs, ~747 cm^{-1}) and larger aggregates (AGGs, ~751 cm^{-1}) (Fig. 3b and c), [35]. At the lowest salt concentration (sample 3S:H_2O:1L, with a concentration of 2.6 mol kg^{-1}), the dominant solvation structure is SSIP (grey band in Fig. 3b), but there still exist a significant population of free sulfolane (cyan band in Fig. 3b) [21]. As the salt concentration increases, the solvation structure undergoes significant modification, with negligible free sulfolane remaining in the most concentrated sample (3S:H_2O:3L, 7.8 mol kg^{-1}). This transition is marked by the transformation of SSIPs, prevalent in dilute concentrations, into CIPs (purple band) and further into AGGs (green band) [36,37]. While any quantitative Raman analysis of the speciation in highly concentrated electrolytes is laden with problems of communal ion solvation [38], as well as differences in the Raman cross-sections, the increase in CIPs and AGGs correlates well with the observed decreased ionic conductivities.

Turning to the 3000-4000 cm^{-1} region, which contains the bands of the water OH stretching modes, we find that the broad band (3200-3450 cm^{-1}) due to hydrogen bonding [39] decreases in intensity with increasing sulfolane content and finally disappears with the addition of Li-salt (Fig. S9). This shows that, as hypothesized, sulfolane reduces the hydrogen bonding network, which is also manifested as a reduced glass transition temperature, as observed in the DSC measurements, attributed to an increase in non-hydrogen bonding water molecules.

4. Conclusions

We believe that the modification of the cation solvation structure via an electrochemically inert co-solvent, such as sulfolane, combined with the use of standard current collectors is a viable strategy to develop next-generation, highly safe, and high-energy aqueous batteries.

To substantiate the proclaimed safety improvements, we performed Accelerated Rate Calorimetry measurements on coin cells that differed only in the electrolyte used; 3S:H_2O:3L *vs.* 1 M $LiPF_6$ in EC-DMC. The measurement has been performed following the protocol in Fig. S10. While any detailed discussion of the degradation mechanism is beyond the scope of this paper, the heating curves (Fig. 4a) show both cells to remain thermally stable up to 180 °C, above which exothermic processes occurred. This similar behavior suggests that the underlying processes likely originate in the electrodes rather than the electrolytes. Notably, as heat is released, the organic electrolyte cell demonstrated a persistent self-heating trend, progressing gradually, possibly towards a thermal runaway. In the cell utilizing the hybrid electrolyte, however, we observe significantly improved behavior. This is primarily due to the heating process automatically shutting down at 200 °C. Following this, the instrument resumes heating mode, yet no heat-generating reactions

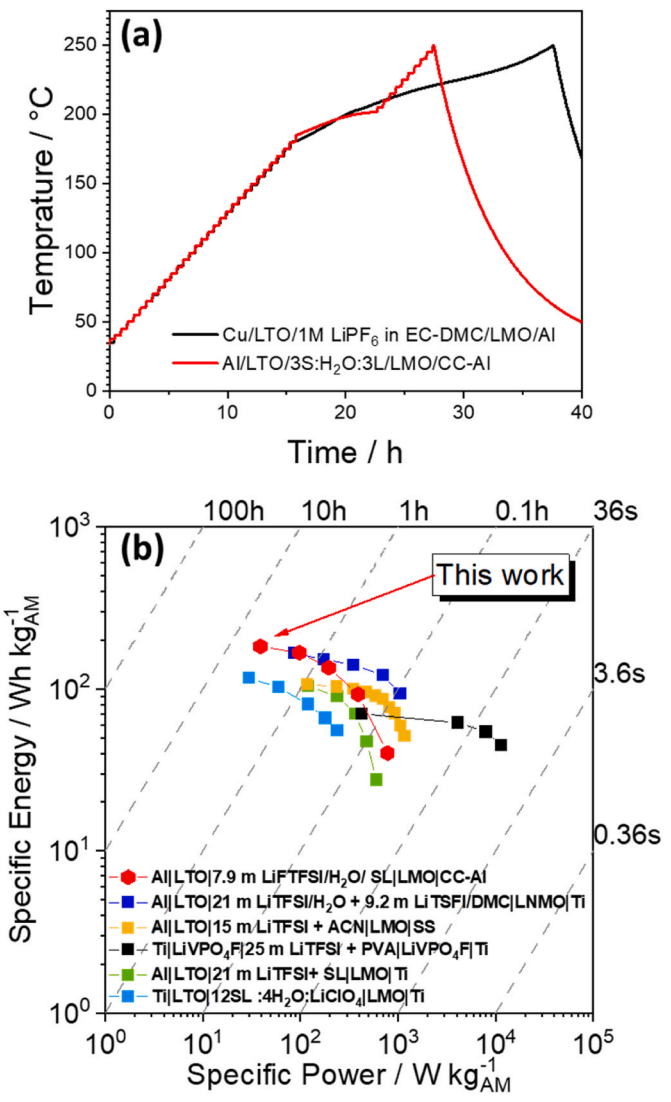

Fig. 4. (a) Comparison between the ARC tests of the Al|LTO|3S:H_2O:3L|LMO|CC-Al and the Al|LTO|1 M $LiPF_6$ in EC:DMC|LMO|CC-Al full coin cell batteries (b), Ragone plot of the Al|LTO|3S:H_2O:3L|LMO|CC-Al full coin cell battery and comparison with similar cells [13,17,21,22,40]. Energy and specific power were normalised to the amount of active material (AM).

are detected until reaching the final temperature. Therefore, we consider the ARC measurement as compelling evidence showcasing the superior stability of our electrolyte when compared to the standard carbonate-based and water-free LIB electrolyte.

Expanding beyond safety considerations, our investigation delves into the energy performance of Al|LTO|3S:H_2O:3L|LMO|CC-Al cell. A Ragone plot (Fig. 4b) encompassing various similar cells and chemistries, based on the total mass of active material at both electrodes, provides compelling insights. Notably, our cell configuration exhibits the highest energy density at low currents and maintains commendable power densities. This underscores the potential of our devised electrolyte system to not only ensure safety but also deliver competitive energy storage performance, positioning it favorably in the landscape of advanced aqueous battery applications.

CRediT authorship contribution statement

Shahid Khalid: Writing – review & editing, Writing – original draft, Methodology, Investigation, Formal analysis, Data curation, Conceptualization. **Ivan Claudio Pellini:** Writing – review & editing, Writing – original draft, Investigation, Formal analysis, Data curation. **Nicolò Pianta:** Writing – review & editing, Methodology, Investigation, Formal analysis, Data curation. **Roberto Lorenzi:** Writing – review & editing, Methodology, Investigation. **Silvia Leonardi:** Writing – review & editing, Validation, Supervision. **Laura Meda:** Writing – review & editing, Supervision. **Caterina Rizzo:** Writing – review & editing, Supervision. **Ernesto Roccaro:** Writing – review & editing. **Patrik Johansson:** Writing – review & editing, Writing – original draft, Supervision, Methodology, Funding acquisition, Conceptualization. **Piercarlo Mustarelli:** Writing – review & editing, Writing – original draft, Validation, Supervision, Methodology, Funding acquisition. **Riccardo Ruffo:** Writing – review & editing, Writing – original draft, Supervision, Project administration, Methodology, Funding acquisition, Data curation, Conceptualization.

Declaration of competing interest

The authors declare that they have no known competing financial interests or personal relationships that could have appeared to influence the work reported in this paper.

Data availability

Data will be made available on request.

Acknowledgements

This work has been financed by Ministry of University and Research (MIUR) through grant “Dipartimenti di Eccellenza - 2017 “Materials for Energy”, and by ENI Spa, under the Joint Research Agreement ENI-University of Milano Bicocca, grant number 5210001818.

This study was carried out within the MOST – Sustainable Mobility Center and received funding from the European Union Next-Generation EU (PIANO NAZIONALE DI RIPRESA E RESILIENZA (PNRR) – MISSIONE 4 COMPONENTE 2, INVESTIMENTO 1.4 – D.D. 1033 June 17, 2022, CN00000023). This manuscript reflects only the authors’ views and opinions, neither the European Union nor the European Commission can be considered responsible for them.

P.J. acknowledges the financial support from the Area of Advance Energy at Chalmers University of Technology to host S.K.

Appendix A. Supplementary data

Supplementary data to this article can be found online at https://doi.org/10.1016/j.jpowsour.2024.234803.

References

[1] W. Tang, Y. Zhu, Y. Hou, L. Liu, Y. Wu, K.P. Loh, H. Zhang, K. Zhu, Aqueous rechargeable lithium batteries as an energy storage system of superfast charging, Energy Environ. Sci. 6 (2013) 2093–2104, https://doi.org/10.1039/C3EE24249H.

[2] C. Wessells, R.A. Huggins, Y. Cui, Recent results on aqueous electrolyte cells, J. Power Sources 196 (2011) 2884–2888, https://doi.org/10.1016/J.JPOWSOUR.2010.10.098.

[3] Y. Wang, J. Yi, Y. Xia, Recent progress in aqueous lithium-ion batteries, Adv. Energy Mater. 2 (2012) 830–840, https://doi.org/10.1002/AENM.201200065.

[4] L. Suo, O. Borodin, T. Gao, M. Olguin, J. Ho, X. Fan, C. Luo, C. Wang, K. Xu, “Water-in-salt” electrolyte enables high-voltage aqueous lithium-ion chemistries, Science 350 (1979) 938–943, https://doi.org/10.1126/SCIENCE.AAB1595, 2015.

[5] L. Suo, O. Borodin, W. Sun, X. Fan, C. Yang, F. Wang, T. Gao, Z. Ma, M. Schroeder, A. von Cresce, S.M. Russell, M. Armand, A. Angell, K. Xu, C. Wang, Advanced high-voltage aqueous lithium-ion battery enabled by “water-in-Bisalt” electrolyte, Angew. Chem. Int. Ed. 55 (2016) 7136–7141, https://doi.org/10.1002/ANIE.201602397.

[6] M.R. Lukatskaya, J.I. Feldblyum, D.G. Mackanic, F. Lissel, D.L. Michels, Y. Cui, Z. Bao, Concentrated mixed cation acetate “water-in-salt” solutions as green and low-cost high voltage electrolytes for aqueous batteries, Energy Environ. Sci. 11 (2018) 2876–2883, https://doi.org/10.1039/C8EE00833G.

[7] D. Chao, W. Zhou, F. Xie, C. Ye, H. Li, M. Jaroniec, S.Z. Qiao, Roadmap for advanced aqueous batteries: from design of materials to applications, Sci. Adv. 6 (2020), https://doi.org/10.1126/SCIADV.ABA4098.

[8] P. Kulkarni, D. Ghosh, R.G. Balakrishna, Recent progress in 'water-in-salt' and 'water-in-salt'-hybrid-electrolyte-based high voltage rechargeable batteries, Sustain. Energy Fuels 5 (2021) 1619–1654, https://doi.org/10.1039/D0SE01313G.
[9] D. Reber, R. Grissa, M. Becker, R.S. Kühnel, C. Battaglia, Anion selection criteria for water-in-salt electrolytes, Adv. Energy Mater. 11 (2021) 2002913, https://doi.org/10.1002/AENM.202002913.
[10] M. Becker, R.-S. Kü, C. Battaglia, R. Li, Chemcomm, C. Communication, Water-in-salt electrolytes for aqueous lithium-ion batteries with liquidus temperatures below −10 °C, Chem. Commun. 55 (2019) 12032–12035, https://doi.org/10.1039/C9CC04495G.
[11] D. Reber, R. Figi, R.S. Kühnel, C. Battaglia, Stability of aqueous electrolytes based on LiFSI and NaFSI, Electrochim. Acta 321 (2019) 134644, https://doi.org/10.1016/J.ELECTACTA.2019.134644.
[12] L. Droguet, A. Grimaud, O. Fontaine, J.M. Tarascon, Water-in-Salt electrolyte (WiSE) for aqueous batteries: a long way to practicality, Adv. Energy Mater. 10 (2020) 2002440, https://doi.org/10.1002/aenm.202002440.
[13] F. Wang, O. Borodin, M.S. Ding, M. Gobet, J. Vatamanu, X. Fan, T. Gao, N. Edison, Y. Liang, W. Sun, S. Greenbaum, K. Xu, C. Wang, Hybrid aqueous/non-aqueous electrolyte for safe and high-energy Li-ion batteries, Joule 2 (2018) 927–937, https://doi.org/10.1016/J.JOULE.2018.02.011.
[14] H. Zhang, B. Qin, J. Han, S. Passerini, Aqueous/nonaqueous hybrid electrolyte for sodium-ion batteries, ACS Energy Lett. 3 (2018) 1769–1770, https://doi.org/10.1021/ACSENERGYLETT.8B00919.
[15] N. Dubouis, A. Serva, E. Salager, M. Deschamps, M. Salanne, A. Grimaud, The fate of water at the electrochemical interfaces: electrochemical behavior of free water versus coordinating water, J. Phys. Chem. Lett. 9 (2018) 6683–6688, https://doi.org/10.1021/ACS.JPCLETT.8B03066/ASSET/IMAGES/LARGE/JZ-2018-03066H_0004.JPEG.
[16] J. Vatamanu, O. Borodin, Ramifications of water-in-salt interfacial structure at charged electrodes for electrolyte electrochemical stability, J. Phys. Chem. Lett. 8 (2017) 4362–4367, https://doi.org/10.1021/ACS.JPCLETT.7B01879/ASSET/IMAGES/LARGE/JZ-2017-018798_0004.JPEG.
[17] J. Chen, J. Vatamanu, L. Xing, O. Borodin, H. Chen, X. Guan, X. Liu, K. Xu, W. Li, Improving electrochemical stability and low-temperature performance with water/acetonitrile hybrid electrolytes, Adv. Energy Mater. 10 (2020) 1902654, https://doi.org/10.1002/AENM.201902654.
[18] P. Jaumaux, X. Yang, B. Zhang, J. Safaei, X. Tang, D. Zhou, C. Wang, G. Wang, Localized water-in-salt electrolyte for aqueous lithium-ion batteries, Angew. Chem. Int. Ed. 60 (2021) 19965–19973, https://doi.org/10.1002/ANIE.202107389.
[19] D. Xiao, Q. Dou, L. Zhang, Y. Ma, S. Shi, S. Lei, H. Yu, X. Yan, Optimization of organic/water hybrid electrolytes for high-rate carbon-based supercapacitor, Adv. Funct. Mater. 29 (2019) 1904136, https://doi.org/10.1002/ADFM.201904136.
[20] Y. Wang, T. Wang, D. Dong, J. Xie, Y. Guan, Y. Huang, J. Fan, Y.C. Lu, Enabling high-energy-density aqueous batteries with hydrogen bond-anchored electrolytes, Matter 5 (2022) 162–179, https://doi.org/10.1016/J.MATT.2021.10.021.
[21] D. Liu, L. Yuan, X. Li, J. Chen, R. Xiong, J. Meng, S. Zhu, Y. Huang, Tuning the electrolyte solvation structure via a nonaqueous Co-solvent to enable high-voltage aqueous lithium-ion batteries, ACS Appl. Mater. Interfaces 14 (2022) 17585–17593, https://doi.org/10.1021/acsami.2c03460.
[22] J. Liu, C. Yang, X. Chi, B. Wen, W. Wang, Y. Liu, Water/sulfolane hybrid electrolyte achieves ultralow-temperature operation for high-voltage aqueous lithium-ion batteries, Adv. Funct. Mater. 32 (2022), https://doi.org/10.1002/ADFM.202106811.
[23] D. Reber, R.-S. Ku, C. Battaglia, Suppressing Crystallization of Water-In-Salt Electrolytes by Asymmetric Anions Enables Low-Temperature Operation of High-Voltage Aqueous Batteries, vol. 14, 2021, p. 26, https://doi.org/10.1021/acsmaterialslett.9b00043.
[24] P.L. Stigliano, N. Pianta, S. Bonizzoni, M. Mauri, R. Simonutti, R. Lorenzi, B. Vigani, V. Berbenni, S. Rossi, P. Mustarelli, R. Ruffo, A physico-chemical investigation of highly concentrated potassium acetate solutions towards applications in electrochemistry, Phys. Chem. Chem. Phys. 23 (2021) 1139–1145, https://doi.org/10.1039/d0cp04151c.
[25] P. Mustarelli, C. Tomasi, Heat capacities of thermally treated Na2O-3B2O3 glasses above and below Tg, Z. Naturforsch. 51 (1996) 187–191, https://doi.org/10.1515/ZNA-1996-0309.
[26] L. Mezzomo, N. Pianta, I. Ostroman, N. Aloni, D. Golodnitsky, E. Peled, P. Mustarelli, R. Ruffo, Deep eutectic solvent electrolytes based on trifluoroacetamide and LiPF6 for Li-metal batteries, J. Power Sources 561 (2023) 232746, https://doi.org/10.1016/J.JPOWSOUR.2023.232746.
[27] Q. Gao, Z. Jian, Measured and ideal glass transition temperatures of glass-forming liquids, J. Mol. Liq. 296 (2019) 111962, https://doi.org/10.1016/J.MOLLIQ.2019.111962.
[28] R.-S. Kühnel, D. Reber, C. Battaglia, Perspective—electrochemical stability of water-in-salt electrolytes, J. Electrochem. Soc. 167 (2020) 070544, https://doi.org/10.1149/1945-7111/AB7C6F.
[29] A. Nakanishi, K. Ueno, D. Watanabe, Y. Ugata, Y. Matsumae, J. Liu, M.L. Thomas, K. Dokko, M. Watanabe, Sulfolane-based highly concentrated electrolytes of lithium bis(trifluoromethanesulfonyl)amide: ionic transport, Li-ion coordination, and Li-S battery performance, J. Phys. Chem. C 123 (2019) 14229–14238, https://doi.org/10.1021/ACS.JPCC.9B02625/ASSET/IMAGES/LARGE/JP-2019-02625J_0011.JPEG.
[30] H.M. Badawi, W. Förner, B. el Ali, A.R.A.H. Al-Durais, Ring inversion, structural stability and vibrational assignments of sulfolane c-C4H8SO2 and 3-sulfolene c-C4H6SO2, Spectrochim. Acta Mol. Biomol. Spectrosc. 70 (2008) 983–990, https://doi.org/10.1016/J.SAA.2007.09.049.
[31] X. Xuan, J. Wang, J. Lu, N. Pei, Y. Mo, Ion solvation and association in LiClO4/sulfolane solution: a vibrational spectroscopic and molecular orbital study, Spectrochim. Acta Mol. Biomol. Spectrosc. 57 (2001) 1555–1560, https://doi.org/10.1016/S1386-1425(00)00486-8.
[32] G.A. Giffin, N. Laszczynski, S. Jeong, S. Jeremias, S. Passerini, Conformations and vibrational assignments of the (fluorosulfonyl) (trifluoromethanesulfonyl)imide anion in ionic liquids, J. Phys. Chem. C 117 (2013) 24206–24212, https://doi.org/10.1021/JP408565B/SUPPL_FILE/JP408565B_SI_001.PDF.
[33] J.E. Katon, W.R. Feairheller, The vibrational spectra and molecular configuration of sulfolane, Spectrochim. Acta 21 (1965) 199–201, https://doi.org/10.1016/0371-1951(65)80117-5.
[34] K. Dokko, D. Watanabe, Y. Ugata, M.L. Thomas, S. Tsuzuki, W. Shinoda, K. Hashimoto, K. Ueno, Y. Umebayashi, M. Watanabe, Direct evidence for Li ion hopping conduction in highly concentrated sulfolane-based liquid electrolytes, J. Phys. Chem. B 122 (2018) 10736–10745, https://doi.org/10.1021/ACS.JPCB.8B09439/SUPPL_FILE/JP8B09439_SI_004.CIF.
[35] X. Gao, F. Wu, A. Mariani, S. Passerini, Concentrated ionic-liquid-based electrolytes for high-voltage lithium batteries with improved performance at room temperature, ChemSusChem 12 (2019) 4185–4193, https://doi.org/10.1002/cssc.201901739.
[36] Y. Yamada, K. Furukawa, K. Sodeyama, K. Kikuchi, M. Yaegashi, Y. Tateyama, A. Yamada, Unusual stability of acetonitrile-based superconcentrated electrolytes for fast-charging lithium-ion batteries, J. Am. Chem. Soc. 136 (2014) 5039–5046, https://doi.org/10.1021/JA412807W/SUPPL_FILE/JA412807W_SI_001.PDF.
[37] A. Boschin, P. Johansson, Characterization of NaX (X: TFSI, FSI) – PEO based solid polymer electrolytes for sodium batteries, Electrochim. Acta 175 (2015) 124–133, https://doi.org/10.1016/J.ELECTACTA.2015.03.228.
[38] G. Åvall, J. Wallenstein, G. Cheng, K.L. Gering, P. Johansson, D.P. Abraham, Highly concentrated electrolytes: electrochemical and physicochemical characteristics of LiPF6 in propylene carbonate solutions, J. Electrochem. Soc. 168 (2021) 050521, https://doi.org/10.1149/1945-7111/ABFDC3.
[39] D.M. Carey, G.M. Korenowski, Measurement of the Raman spectrum of liquid water, J. Chem. Phys. 108 (1998) 2669, https://doi.org/10.1063/1.475659.
[40] C. Yang, X. Ji, X. Fan, T. Gao, L. Suo, F. Wang, W. Sun, J. Chen, L. Chen, F. Han, L. Miao, K. Xu, K. Gerasopoulos, C. Wang, C. Yang, X. Ji, X. Fan, T. Gao, L. Suo, F. Wang, W. Sun, J. Chen, L. Chen, F. Han, C. Wang, L. Miao, K. Xu, K. Gerasopoulos, Flexible aqueous Li-ion battery with high energy and power densities, Adv. Mater. 29 (2017) 1701972, https://doi.org/10.1002/ADMA.201701972.